

# TeSG: Textual Semantic Guidance for Infrared and Visible Image Fusion

Mingrui Zhu  
Xidian University  
mrzhu@xidian.edu.cn

Xiru Chen  
Xidian University  
xrchen@stu.xidian.edu.cn

Xin Wei  
Xidian University  
weixin@xidian.edu.cn

Nannan Wang  
Xidian University  
nnwang@xidian.edu.cn

Xinbo Gao  
Chongqing University of Post and Telecommunications  
gaoxb@cqupt.edu.cn

## Abstract

Infrared and visible image fusion (IVF) aims to combine complementary information from both image modalities, producing more informative and comprehensive outputs. Recently, text-guided IVF has shown great potential due to its flexibility and versatility. However, the effective integration and utilization of textual semantic information remains insufficiently studied. To tackle these challenges, we introduce textual semantics at two levels: the mask semantic level and the text semantic level, both derived from textual descriptions extracted by large Vision-Language Models (VLMs). Building on this, we propose **Textual Semantic Guidance for infrared and visible image fusion**, termed **TeSG**, which guides the image synthesis process in a way that is optimized for downstream tasks such as detection and segmentation. Specifically, **TeSG** consists of three core components: a **Semantic Information Generator (SIG)**, a **Mask-Guided Cross-Attention (MGCA)** module, and a **Text-Driven Attentional Fusion (TDAF)** module. The **SIG** generates mask and text semantics based on textual descriptions. The **MGCA** module performs initial attention-based fusion of visual features from both infrared and visible images, guided by mask semantics. Finally, the **TDAF** module refines the fusion process with gated attention driven by text semantics. Extensive experiments demonstrate the competitiveness of our approach, particularly in terms of performance on downstream tasks, compared to existing state-of-the-art methods.

## 1. Introduction

Due to hardware constraints and the inherent limitations of imaging technologies, single-modal sensors often fail to capture all the relevant information in complex scenes. Infrared images excel in low-light or challenging conditions, offering strong thermal radiation detection, but they

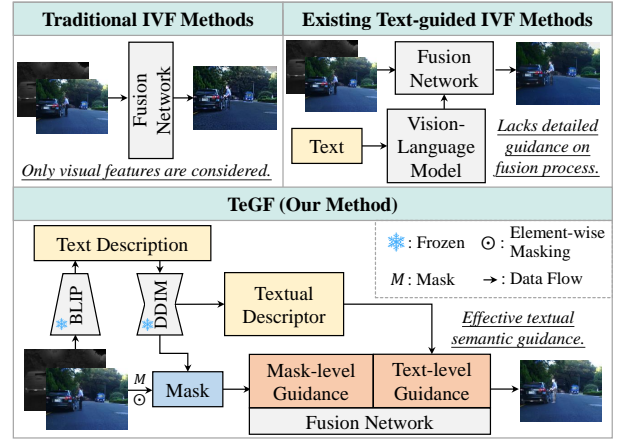


Figure 1. Comparison of existing IVF methods with our TeSG. Traditional methods focus only on low-level image features, while current text-guided IVF methods often overlook intrinsic details during the fusion process. In contrast, our approach combines mask-level, text-level, and image-level features to effectively guide the fusion process.

lack fine details. On the other hand, visible images provide rich texture details but struggle in low-light or low-contrast environments. As a result, neither modality alone can offer a comprehensive and accurate description of a scene [34, 54]. Infrared and visible image fusion (IVF) is a crucial technique for leveraging the complementary strengths of both. The primary goal of IVF is to preserve the thermal characteristics of infrared images while retaining the texture details of visible images, resulting in high-quality fused images. These fused images, with enhanced scene representation, find wide-ranging applications in object detection [10, 13], scene understanding [50], remote sensing [23], and other vital domains.

Over the past few decades, many studies have tackled the challenges of IVF. Traditional methods rely on tech-

niques like multi-scale transformations [27, 33], sparse representation [20, 22], subspace [9, 45], and saliency detection [6, 28] to directly combine multimodal information. While effective to some extent, these methods rely on fixed feature extraction and manually designed fusion rules, which limit their ability to handle complex and diverse scenarios. Recently, deep learning techniques like autoencoders (AE) [21, 29, 53, 56], convolutional neural networks (CNN) [32, 48, 49], generative adversarial networks (GAN) [30, 35–38], and transformers [39, 47] have significantly improved fusion quality through end-to-end learning. However, these methods focus mainly on visual features and often overlook high-level semantic information and scene context. In complex scenarios, this lack of semantic guidance results in reduced semantic consistency and comprehension, leading to suboptimal fusion performance.

Most recently, with the revolution in large vision-language models (VLMs), text-guided IVF [8, 44, 51, 59] has garnered significant attention. TextIF [51] introduces a semantic interaction-guided module that leverages text to specify the types of image degradation, enabling degradation-aware fusion. Zhao *et al.* [59] employs Vision-Language Models (VLMs) to generate detailed semantic descriptions of source images, such as image captions and dense captions, to guide and enhance the fusion of visual features. While the integration of textual information has undoubtedly enhanced the flexibility and performance of existing methods, these approaches still have notable limitations. First, the deep semantic relationship between textual and visual features remains insufficiently explored, with a lack of comprehensive cross-modal interaction and fusion. Second, the precise guidance of textual semantics for effective feature alignment is still largely unaddressed.

To address this issue, we introduce textual semantic guidance, termed TeSG, to effectively steer the fusion process in a manner better aligned with higher-level tasks. TeSG utilizes the pre-trained BLIP model [26] to automatically extract textual descriptions of images, thereby eliminating the complexity of manually inputting text. The guidance provided by these textual descriptions during the image fusion process occurs in two key ways: first, by generating mask semantics for key targets based on the textual descriptions, enabling precise mask-level guidance for fusing visual features in critical regions; and second, by leveraging text semantics (feature embeddings of textual descriptions) to establish semantic correlations with visual features, facilitating textual semantic-level gated filtering and guidance for visual feature fusion. To achieve these objectives, TeSG incorporates three functional modules: the Semantic Information Generator (SIG), the Mask-Guided Cross-Attention (MGCA) module, and the Text-Driven Attentional Fusion (TDAF) module. In this way, TeSG ef-

fectively leverages textual information and provides a more efficient approach to textual semantic guidance compared to existing text-guided IVF methods, as illustrated in Fig. 1. Our contributions are summarized below:

- We explore the potential of using textual descriptions of images to guide the image fusion process and propose an effective textual semantic guidance method. This approach facilitates image fusion through both mask-level and semantic-level guidance, without the need for manual text input.
- We design three closely related modules to implement textual semantic guidance, including a semantic information generator, a mask-guided cross-attention module, and a text-driven attentional fusion module.
- Qualitative and quantitative experiments demonstrate that our method yields higher-quality results, featuring more precise fusion edges and greater information gain, underscoring its effectiveness in supporting higher-level tasks.

## 2. Related Work

### 2.1. Infrared and Visible Image Fusion

Recent advances in deep learning have significantly promoted the development of infrared and visible image fusion (IVF). Current deep learning-based fusion methods can be further divided into the following four categories. Autoencoder (AE)-based methods [21, 24, 29, 53] use encoder-decoder frameworks for feature extraction and image reconstruction. For example, DenseFuse [21] integrates an encoder-decoder network with densely connected convolutional blocks for feature extraction, employing manually designed fusion strategies to integrate features. RFNest [24] proposes an end-to-end residual fusion network, adopting a two-stage training strategy for more effective image fusion. Convolutional Neural Network (CNN)-based methods [32, 39, 48, 49] leverage meticulously designed network architectures and loss functions to extract, integrate, and reconstruct image features. RFNet [49] introduces an unsupervised network for multimodal image registration and fusion, utilizing a mutual reinforcement framework to improve fusion performance. Generative Adversarial Network (GAN)-based methods [30, 35, 37] have gained attention due to their robust ability in unsupervised distribution learning. GANs [12, 40] have demonstrated outstanding performance in infrared and visible image fusion tasks. For instance, FusionGAN [35] employs a generator-discriminator framework to achieve high-quality fusion while effectively preserving fine details. Diffusion-based methods have also emerged as a recent breakthrough in deep learning for image fusion. DDFM [58] utilizes a denoising diffusion probabilistic model for unconditional image generation, excelling in preserving cross-modal information. Similarly, Dif-fusion [52] employs a diffusion

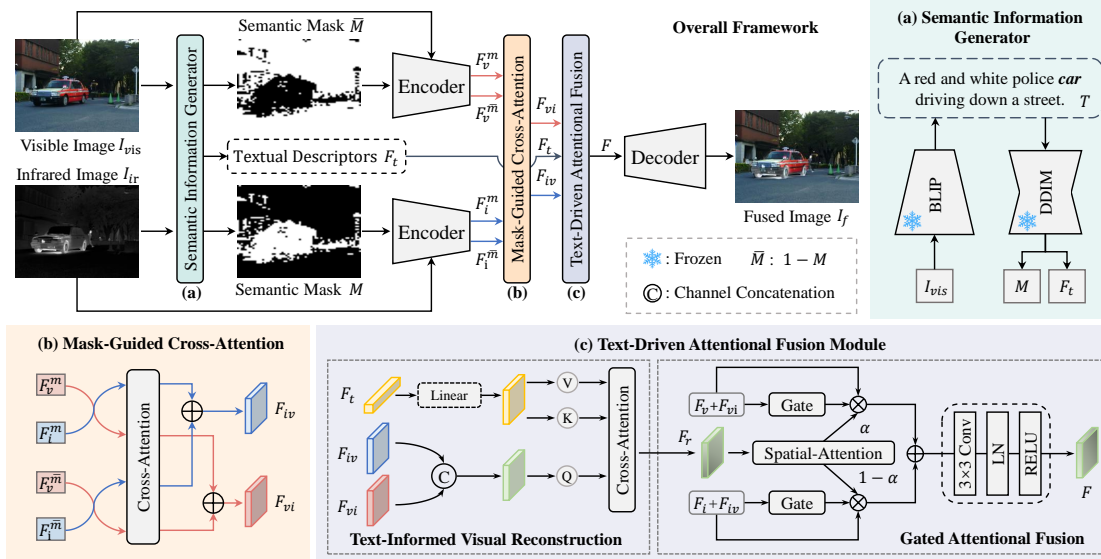


Figure 2. The overall framework of TeSG consists of three primary modules: (a) the Semantic Information Generator (SIG), responsible for generating both mask semantics and text semantics; (b) the Mask-Guided Cross-Attention (MGCA) module, which enables effective cross-modal feature integration through mask-guided attention mechanisms; and (c) the Text-Driven Attentional Fusion (TDAF) module, refining the fusion process by applying gated attention mechanisms driven by the extracted text semantics.

model to directly generate the distribution of multi-channel input data, enhancing the aggregation of multi-source information and improving color fidelity.

## 2.2. Text-guided IVF

Existing methods primarily prioritize the visual quality of fused images, with limited attention given to incorporating semantic information. Some studies attempt to enhance the fused images by integrating downstream tasks, such as object detection [30] and semantic segmentation [31, 42]. But these methods are often task-specific and do not facilitate comprehensive interaction or provide fine-grained control over multimodal features, limiting their effectiveness in more general applications. Text-guided methods, on the other hand, directly integrate textual information into IVF tasks. TextIF [51] proposes a method that combines an image fusion pipeline with a semantic interaction guidance module to perform perceptual and interactive image fusion tasks on degraded images. Zhao *et al.* [59] introduced VLMs into the image fusion domain, using multi-level textual prompts, such as image captions and dense captions, to guide and enhance the fusion of visual features. TeRF [44] presents a flexible image fusion framework with multiple VLMs, enabling text-driven and region-aware image fusion through the parsing of textual instructions. Text-Fusion [8] introduces a text-visual association mapping and an affine fusion unit to achieve fine-grained control over the image fusion process. While existing methods have enhanced fusion quality and model flexibility, they still en-

counter challenges such as high computational complexity and insufficient exploration of deep semantic correlations between textual and visual features. To address these limitations, we propose an efficient text-guided fusion method that facilitates deep multimodal feature integration through dual-level guidance at both the mask and semantic levels, without requiring manually inputted text.

## 3. Method

### 3.1. Overview

Given paired samples  $\{(I_{vis}, I_{ir})_i\}_{i=1}^N$ , where  $I_{vis} \in \mathbb{R}^{H \times W \times 3}$  represents samples from a visible image domain and  $I_{ir} \in \mathbb{R}^{H \times W \times 1}$  represents samples from an infrared image domain, our goal is to learn a parameterized mapping  $I_f = \mathcal{G}(I_{vis}, I_{ir} | \theta)$ . This mapping enables the generation of a high-fidelity fused image that effectively combines the complementary strengths of both sources. To achieve this, we propose Textual Semantic Guidance (TeSG), a method that effectively directs the fusion process in a way that is better aligned with higher-level tasks. TeSG consists of three key components: the Semantic Information Generator (SIG) module (as described in Sec. 3.2), the Mask-Guided Cross-Attention (MGCA) module (as described in Sec. 3.3), and the Text-Driven Attentional Fusion (TDAF) module (as described in Sec. 3.4).

As illustrated in Fig. 2, the aligned visible image  $I_{vis}$  and infrared image  $I_{ir}$  are first processed by the SIG module, where a frozen BLIP encoder [26] extracts textual de-

scriptions from  $I_{vis}$ . These textual descriptions, along with the input images, are then used in a frozen DDIM sampler [41] to generate mask semantics  $M$  and text semantics  $F_t$ . Following this, both input images and their corresponding mask semantics  $M$  are passed through encoders to produce feature representations, including global features (*i.e.*,  $F_v, F_i$ ) and local features (*i.e.*,  $F_v^m, F_v^{\bar{m}}, F_i^m, F_i^{\bar{m}}$ ). Transformer-based blocks are used for both the encoders and the decoder. These encoded features are then processed by the MGCA module, which facilitates cross-modal feature integration through mask-guided attention mechanisms. The resulting features are passed into the TDAF module, where the text semantics  $F_t$  play a crucial role in guiding the image fusion process. Additionally, the TDAF module incorporates a dynamic gating mechanism that adjusts fusion weights to ensure an optimal combination of the visible and infrared image features. Finally, the fused image  $I_f$  is reconstructed through the decoder. We adopt commonly used losses for training, including structural similarity loss, gradient loss, intensity loss, and color loss. Detailed formulations are presented in Sec. A of the supplementary material.

### 3.2. Semantic Information Generator

**Textual Description Generation.** To generate a contextually accurate textual description of the input images, we leverage the pre-trained BLIP model [26]. The visible image  $I_{vis}$  is passed through the frozen BLIP encoder to produce a corresponding textual description  $T$ . This process can be expressed as:

$$T = \text{BLIP}(I_{vis}), \quad (1)$$

where  $I_{vis}$  represents the input visible image, and  $T$  denotes the generated textual description that captures the key semantic content of the image, as inferred by the BLIP model. Additionally, we modify  $T$  by removing the keyword  $V^*$ , resulting in the modified textual description  $\hat{T}$ . Specifically, the keyword  $V^*$  (*e.g.*, “car” in Fig. 3) is defined as the term that corresponds to key objects in high-level tasks, such as object detection and scene segmentation.

**Mask Semantics Generation.** One of the persistent challenges in IVF tasks is managing information redundancy and preventing the loss of critical details during the fusion process. To address these issues, we introduce mask semantics designed to emphasize the complementary features between infrared and visible modalities. Specifically, we propose a noise-based strategy where Gaussian noise is added to the input visible image,  $I_{vis}$ , and the resulting noisy image is processed under two distinct textual conditions (*i.e.*,  $T$  and  $\hat{T}$ ) within the diffusion model. This approach enables us to investigate how variations in text influence information within specific regions. The mask is then inferred by evaluating the difference in noise estimation produced by

the diffusion model under these two textual conditions. This process can be expressed as:

$$M_{vis} = \Delta(D_\theta(I_{vis}, T) - D_\theta(I_{vis}, \hat{T})), \quad (2)$$

where  $D_\theta$  represents the diffusion model, and  $\Delta$  denotes the normalization and binarization of the computed noise difference. To further mitigate the challenge of insufficient information extraction from individual modalities, we extend this approach to both visible and infrared images. Specifically, we generate masks  $M_{vis}$  and  $M_{ir}$  for the visible image  $I_{vis}$  and the infrared image  $I_{ir}$ , respectively, and then take their union to obtain the final mask semantics  $M$ :

$$M = M_{vis} \cup M_{ir}. \quad (3)$$

**Text Semantics Generation.** The text encoder of the diffusion model converts the textual description  $T$  into an embedding vector  $F_t$ , which serves as the text semantics. Overall, the SIG produces both mask-level and text-level semantics to guide the subsequent fusion process.

### 3.3. Mask-Guided Cross-Attention

The MGCA module first utilizes mask semantics to decompose the images into key target foreground images and background images. Given the visible image  $I_{vis}$ , the infrared image  $I_{ir}$ , and the corresponding mask semantics  $M$ , the module applies both the foreground semantics  $M$  and the background semantics  $\bar{M}$  to each input image, where  $\bar{M}$  is defined as the complementary regions of the foreground mask. This results in four distinct masked images that capture both foreground and background information for each modality. These masked images are then passed through an encoder to extract their initial feature representations, denoted as  $F_v^m, F_v^{\bar{m}}, F_i^m$  and  $F_i^{\bar{m}}$ , where the superscripts  $m$  and  $\bar{m}$  indicate the foreground and background features, respectively.

Subsequently, we perform feature reconstruction based on cross-attention for the foreground and background features of both visible and infrared images. The foreground and background features of the infrared image,  $F_i^m$  and  $F_i^{\bar{m}}$ , are used to reconstruct the foreground and background features of the visible image,  $F_v^m$  and  $F_v^{\bar{m}}$ , resulting in  $F_{vi}^m$  and  $F_{vi}^{\bar{m}}$ :

$$F_{vi}^m = CA(F_v^m, F_i^m), \quad F_{vi}^{\bar{m}} = CA(F_v^{\bar{m}}, F_i^{\bar{m}}); \quad (4)$$

conversely, the foreground and background features of the visible image,  $F_v^m$  and  $F_v^{\bar{m}}$ , are used to reconstruct the foreground and background features of the infrared image,  $F_i^m$  and  $F_i^{\bar{m}}$ , resulting in  $F_{iv}^m$  and  $F_{iv}^{\bar{m}}$ :

$$F_{iv}^m = CA(F_i^m, F_v^m), \quad F_{iv}^{\bar{m}} = CA(F_i^{\bar{m}}, F_v^{\bar{m}}), \quad (5)$$

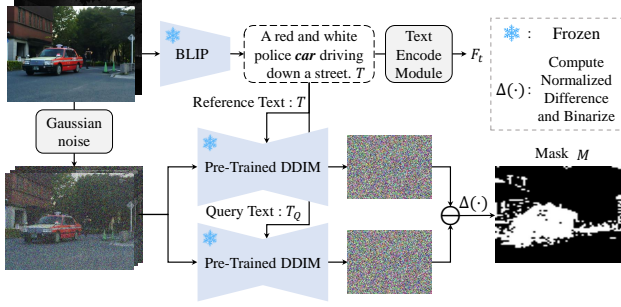


Figure 3. The process of the Semantic Information Generator.

where  $CA$  denotes the cross-attention mechanism. Finally, the corresponding features are summed element-wise to obtain the fully reconstructed visible and infrared features:

$$F_{vi} = F_{vi}^m + \overline{F_{vi}^m}, \quad F_{iv} = F_{iv}^m + \overline{F_{iv}^m}. \quad (6)$$

### 3.4. Text-Driven Attentional Fusion

**Text-Informed Visual Reconstruction.** Given the reconstructed visible and infrared features,  $F_{vi}$  and  $F_{iv}$ , along with the text semantics  $F_t$ , the features  $F_{vi}$  and  $F_{iv}$  are first concatenated to form the multimodal visual features. The multimodal visual features are then reconstructed using  $F_t$  through the cross-attention mechanism, enabling effective feature interaction. This process is formally defined as follows:

$$F_r = CA(Cat(F_{vi}, F_{iv}), F_t), \quad (7)$$

where  $Cat(\cdot)$  represents the concatenation of features and  $CA$  denotes the cross-attention mechanism. Through this process, the module generates the text-informed multimodal visual features  $F_r$ , which integrate text semantic information with multimodal features.

**Gated Attentional Fusion.** To fully leverage the complementary characteristics of infrared and visible features, we introduce a gated mechanism that dynamically weights and fuses the two modalities. First, the reconstructed visible and infrared features,  $F_{vi}$  and  $F_{iv}$ , are added to the initial image features,  $F_v$  and  $F_i$ , respectively. The resulting features are then processed through a convolutional layer to generate the gating weights,  $G_v$  and  $G_i$ . The gating weights are computed as follows:

$$\begin{aligned} G_v &= \sigma(W_v \cdot (F_v + F_{vi})), \\ G_i &= \sigma(W_i \cdot (F_i + F_{iv})), \end{aligned} \quad (8)$$

where  $\sigma$  denotes the Sigmoid activation function, and  $W_v$  and  $W_i$  represent the weight matrices of the convolutional layers for the visible and infrared features, respectively. These gating weights control the contribution of each modality to the final fused representation. Subsequently,

spatial attention weights are derived from the text-informed multimodal visual features  $F_r$ , using a Multilayer Perceptron (MLP) for feature refinement:

$$\alpha = SA(F_r) = \sigma(\Phi_{SA}(F_r)), \quad (9)$$

where  $\Phi_{SA}$  is a fusion function implemented as a MLP consisting of a two-layer convolutional block with a ReLU activation. Finally, the spatial attention weight  $\alpha$  and gating weights  $G_v$  and  $G_i$  are jointly applied to adaptively weight and fuse the infrared and visible features. This fusion process is defined as:

$$F = \alpha \cdot (1 + G_v) \cdot (F_v + F_{vi}) + (1 - \alpha) \cdot (1 + G_i) \cdot (F_i + F_{iv}), \quad (10)$$

where  $F$  denotes the final fused feature, which is then passed through the decoder to generate the high-quality fused image  $I_f$ .

## 4. Experiments

### 4.1. Experimental Setting

**Implementation Details.** Our method is implemented in PyTorch and trained across four 24GB NVIDIA GeForce RTX 3090 GPUs. For training, we utilize the AdamW optimizer with an initial learning rate of 0.0001, conducting 140 epochs with a batch size of 8. Training samples are randomly cropped into  $96 \times 96$  patches. The model architecture consists of two encoders and a decoder, each comprising four transformer blocks.

**Datasets.** Our experiments utilize three publicly available datasets: MSRS [43], RoadScene [48], and LLVIP [16]. The model is trained on the MSRS dataset and evaluated on the RoadScene and LLVIP datasets. The MSRS dataset contains 1,083 training pairs of infrared and visible images, and 361 test pairs. For evaluation, we use 221 image pairs from the RoadScene dataset and 347 randomly selected image pairs from the LLVIP dataset to assess the generalization capabilities of the model across different environments.

**Compared Methods.** We compare our method with nine state-of-the-art (SOTA) approaches: TarDAL [30], ReCoNet [15], LRRNet [25], MetaFusion [55], CDDFuse [57], DDFM [58], Text-IF [51], TextFusion [8], and MMDRFuse [11].

**Evaluation Metrics.** To quantitatively assess the performance of the proposed fusion model, we adopt five widely used metrics that evaluate various aspects of the fused image quality. These include: Entropy (EN) [34], which measures the amount of information retained in the fused image; Standard Deviation (SD), which reflects the richness of information and contrast in the fused image; the Sum of the Correlations of Differences (SCD) [5], which assesses the similarity between the fused and source images; Visual Information Fidelity (VIF) [14], which quantifies the amount



Figure 4. Qualitative comparison of our method against nine state-of-the-art (SOTA) methods. The images, arranged from top to bottom, are sourced from the MSRS, RoadScene, and LLVIP datasets.

of visual information shared between the fused and source images—higher VIF values indicate better alignment with human visual perception; and  $Q^{AB/F}$  [34], which evaluates the preservation of edge information from the source images. Higher values across these metrics indicate better performance of the image fusion method.

## 4.2. Comparison with SOTA Fusion Methods

### Qualitative Comparison.

We present a qualitative comparative analysis of the proposed method against nine state-of-the-art (SOTA) fusion methods on the MSRS [43], RoadScene [48], and LLVIP [16] datasets, as shown in Fig. 4. The results highlight notable limitations in existing methods. TarDAL, ReCoNet, and LRRNet fail to adequately preserve both infrared and visible information, causing significant information loss (*e.g.*, pedestrians marked by red boxes in MSRS and LLVIP datasets appear indistinct). LRRNet retains

some texture details, but TarDAL and ReCoNet struggle with these details (*e.g.*, the ground text marked by red boxes in RoadScene dataset appears blurred). TextFusion and MetaFusion show better retention of image details but still have limitations. TextFusion fails to clearly highlight thermal targets (*e.g.*, thermal targets in red boxes are not distinct), and MetaFusion shows noticeable color distortion, with both methods producing images of lower brightness. MMDRFuse and DDFM produce low-contrast images, where the overall colors resemble single-modality images, failing to integrate infrared and visible information effectively and making thermal targets less prominent. CDDFuse and Text-IF generate relatively higher-quality images, preserving infrared information well. However, they blur key visible image texture details, with Text-IF occasionally introducing color distortion (*e.g.*, the background marked by blue boxes in MSRS dataset). In contrast, our proposed TeSG method, with its effective textual seman-

Methods	MSRS Dataset					RoadScene Dataset					LLVIP Dataset				
	EN $\uparrow$	SD $\uparrow$	SCD $\uparrow$	VIF $\uparrow$	$Q^{AB/F} \uparrow$	EN $\uparrow$	SD $\uparrow$	SCD $\uparrow$	VIF $\uparrow$	$Q^{AB/F} \uparrow$	EN $\uparrow$	SD $\uparrow$	SCD $\uparrow$	VIF $\uparrow$	$Q^{AB/F} \uparrow$
TarDAL	5.322	23.346	0.697	0.406	0.172	7.259	47.897	1.435	0.546	0.396	6.322	37.047	1.030	0.526	0.211
ReCoNet	4.234	41.714	1.262	0.490	0.404	7.054	41.275	1.536	0.545	0.380	5.800	46.898	1.461	0.559	0.405
LRRNet	6.192	31.758	0.791	0.542	0.454	7.132	42.436	1.569	0.494	0.352	6.381	29.189	0.869	0.547	0.420
MetaFusion	6.357	39.133	1.502	0.686	0.464	<u>7.391</u>	50.749	1.549	0.527	0.402	7.042	46.631	1.327	0.623	0.293
CDDFuse	<u>6.701</u>	<u>43.374</u>	1.621	<u>1.051</u>	0.693	<b>7.453</b>	<b>56.322</b>	1.712	0.624	0.483	7.342	49.971	<u>1.580</u>	0.880	0.642
DDFM	6.175	28.922	1.449	0.743	0.474	7.250	43.188	<u>1.713</u>	0.571	0.407	7.089	40.374	1.417	0.648	0.258
Text-IF	6.665	43.190	<u>1.689</u>	1.049	<u>0.716</u>	7.319	49.871	1.522	<u>0.686</u>	<b>0.591</b>	<b>7.428</b>	<u>50.250</u>	1.444	<u>1.033</u>	<u>0.747</u>
TextFusion	6.029	38.022	1.432	0.722	0.521	7.004	39.752	1.537	0.677	0.397	6.552	38.248	1.278	0.689	0.493
MMDRFuse	6.475	37.323	1.532	0.851	0.591	6.505	27.631	1.102	0.545	0.320	7.245	44.390	1.475	0.812	0.586
<b>Ours</b>	<b>6.712</b>	<b>43.472</b>	<b>1.719</b>	<b>1.080</b>	<b>0.733</b>	7.180	<u>53.678</u>	<b>1.741</b>	<b>0.690</b>	<u>0.577</u>	<u>7.396</u>	<b>52.553</b>	<b>1.614</b>	<b>1.059</b>	<b>0.763</b>

Table 1. Quantitative comparison of our method against nine state-of-the-art (SOTA) methods on the MSRS, LLVIP, and RoadScene datasets. The bolded values indicate the best performance, while underlined values represent the second-best.

tic guidance and gating mechanism, significantly enhances foreground thermal targets while better preserving visible texture details and achieving more realistic brightness. It also presents higher contrast and maintains good contour information and scene details, even under low-light conditions. Our method achieves a balanced fusion of infrared and visible information, delivering higher-quality fusion results both during the day and at night.

**Quantitative Comparison.** Tab. 1 presents the quantitative evaluation results across three datasets using five metrics. Our method outperforms others on MSRS and LLVIP datasets, particularly excelling on MSRS, where it achieves the highest scores across all metrics. The optimal SD, SCD, and VIF scores indicate that our fused images preserve richer structural and texture information from the source images, demonstrating superior fusion effects in both color and detail. This suggests that our model not only enhances semantic consistency in target regions but also ensures the retention of key features from each modality, while maintaining the overall information richness. Notably, the  $Q^{AB/F}$  score shows that our method effectively preserves complementary multimodal features, particularly in retaining edge information, which enhances contrast and contour clarity. Additionally, our method achieves the second-best result in EN, further validating its ability to integrate multi-source information. Overall, our proposed TeSG delivers exceptional performance across multiple datasets, highlighting its strong generalization ability and superior image fusion quality.

### 4.3. Performance on High-level Tasks

To comprehensively evaluate the performance of the fused images on downstream high-level vision tasks, we conduct a systematic analysis of various fusion methods on the MSRS dataset [43] for both object detection and semantic segmentation.

**Evaluation on the Object Detection Task.** YOLOv8<sup>1</sup> is employed as the object detection network to ensure a fair qualitative and quantitative comparison. The results are shown in Fig. 5 and Tab. 2.

The qualitative results in Fig. 5 demonstrate that our method accurately detects all targets in the scene, significantly improving object detection performance and outperforming existing methods. Compared to others, TeSG shows a clear advantage in detection accuracy. For instance, CDDFuse and MMDRFuse incorrectly classify “person” as “bike”, while TextFusion struggles with recognizing the “person” category, highlighting its limitations in preserving key thermal features. Additionally, methods like TarDAL, ReCoNet, and DDFM suffer from missed detections due to their inability to capture critical image details, resulting in lower detection performance. In contrast, our method effectively integrates the infrared and visible information, adequately preserving essential features from both modalities. By leveraging the rich semantic information, our method enhances the model’s ability to understand and identify scene targets. In challenging scenarios with complex backgrounds, it delivers clearer target contours and richer contextual information, improving detection accuracy and stability.

For quantitative evaluation, we use five metrics, including precision, recall, and mean average precision (mAP) at different thresholds. As shown in Tab. 2, our method achieves the highest mAP score, notably outperforming others. Even under rigorous metrics such as mAP@0.75 and mAP@0.5:0.95, TeSG demonstrates superior performance in high-precision object detection tasks. These results highlight our method’s superior performance and robustness under stringent detection requirements.

**Evaluation on the Semantic Segmentation Task.** To further evaluate the performance of our method in semantic segmentation, we select DeeplabV3+ [7] as the backbone

<sup>1</sup><https://github.com/ultralytics/ultralytics>

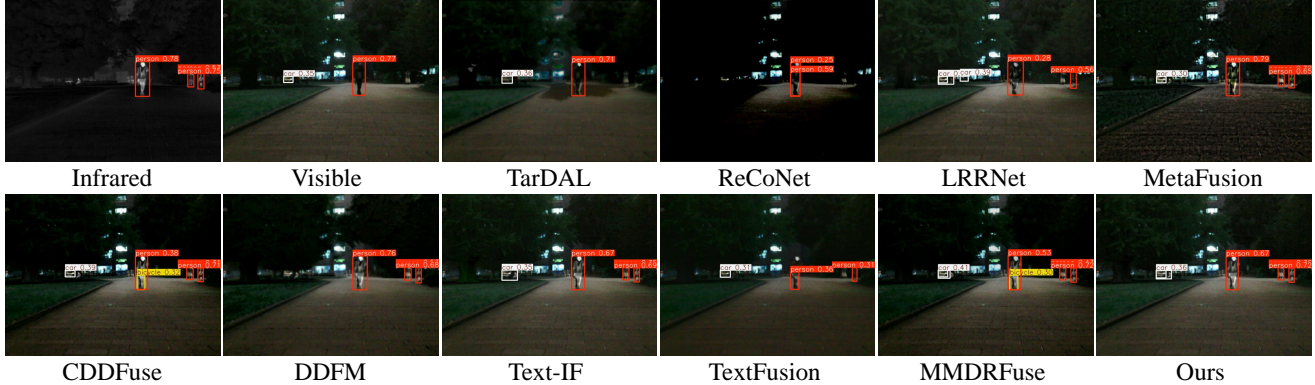


Figure 5. Qualitative comparison of object detection performance on the MSRS dataset.

Methods	mAP $\uparrow$			Precision $\uparrow$	Recall $\uparrow$
	@0.50	@0.75	@0.50:0.95		
TarDAL	0.850	0.597	0.553	0.891	0.744
ReCoNet	0.715	0.526	0.466	0.914	0.622
LRRNet	0.921	0.735	0.674	<b>0.971</b>	0.852
MetaFusion	0.905	0.728	0.647	0.905	0.855
CDDFuse	<u>0.942</u>	0.778	0.684	0.895	<b>0.881</b>
DDFM	<u>0.923</u>	<u>0.818</u>	0.699	0.940	0.835
Text-IF	0.939	0.808	<u>0.709</u>	0.947	0.860
TextFusion	0.861	0.636	0.598	0.888	0.748
MMDRFuse	0.914	0.782	0.688	0.915	0.820
<b>Ours</b>	<b>0.945</b>	<b>0.820</b>	<b>0.717</b>	<u>0.948</u>	<u>0.879</u>

Table 2. Quantitative comparison of object detection performance on the MSRS dataset. The bolded values indicate the best performance, while underlined values represent the second-best.

network and train it on the MSRS dataset, which includes nine categories: background, car, person, bike, curve, car stop, guardrail, color cone, and bump. The model is trained using CrossEntropyLoss with an initial learning rate of 0.01 for 370 epochs and a batch size of 4. The qualitative and quantitative results are presented in Fig. 6 and Tab. 3.

The qualitative results shown in Fig. 6 indicate that our method accurately segments all semantic targets in the scene, delivering superior performance. In contrast, TarDAL performs poorly in detecting distant targets (*e.g.*, the person and bike marked by red boxes), failing to segment these objects correctly. Methods like ReCoNet, LRRNet, MetaFusion, CDDFuse, TextFusion, and MMDRFuse fail to retain sufficient semantic information in the bump area of the fused images (*e.g.*, the bump marked by green boxes), resulting in its missegmentation. While DDFM and Text-IF successfully identify and segment all targets, they exhibit blurred and imprecise boundaries due to inaccurate edge segmentation. In comparison, our method excels by maintaining consistent edge gradient information. By optimizing edge details in the fusion image, we ensure the edges

are highly consistent with those in the input images, enhancing the contrast and clarity of the contours. This significantly improves the performance of our method in downstream tasks like semantic segmentation, further enhancing its practical applicability.

In the quantitative evaluation in Tab. 3, our method achieves the highest mIoU scores. Our approach outperforms other methods across almost all categories, underscoring its superiority in image segmentation tasks. Specifically, our method effectively emphasizes foreground objects while preserving crucial texture details, giving it a strong advantage in both fusion quality and semantic consistency.

#### 4.4. Ablation Study

To assess the contribution of each module to the model’s overall performance, we perform ablation experiments on LLVIP [16] dataset, with the quantitative results provided in Tab. 4.

**Effectiveness of the Mask-Guided Cross-Attention (MGCA) Module.** To validate the effectiveness of the MGCA module, we set up a variant of the module that no longer uses mask semantics to decompose the input images into key target foreground and background regions. Instead, it directly performs feature reconstruction of the entire image using cross-attention. As shown in Tab. 4 (a), most metrics exhibit a decline, while VIF shows a slight increase; however, this improvement is marginal and insufficient to compensate for the overall performance drop. This suggests that mask semantics play a crucial role in the fusion process of TeSG, especially for guiding the fusion and preserving image contrast and edge information. The drop in SD and SCD further indicates that the masks effectively reduce information loss and improving fusion quality.

**Effectiveness of the Text-Informed Visual Reconstruction (TIVR) Module.** To verify the role of text semantics, we remove the TIVR module, eliminating the guidance of text features, and directly fuse the concatenated image fea-

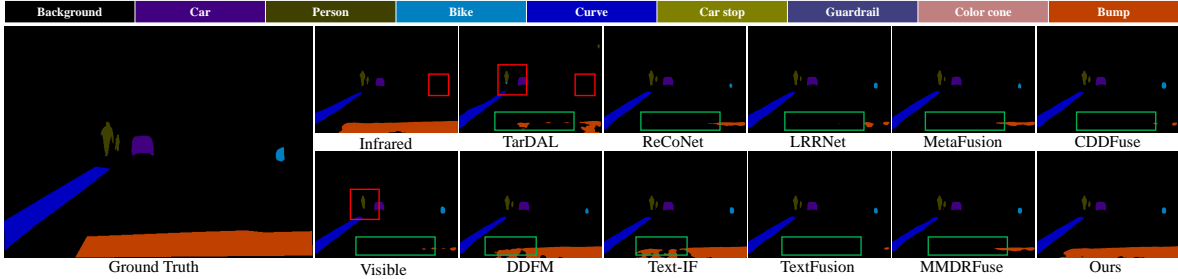


Figure 6. Qualitative comparison of semantic segmentation performance on the MSRS dataset.

Methods	IoU $\uparrow$									
	Background	Car	Person	Bike	Curve	Car stop	Guardrail	Color cone	Bump	mIoU
Infrared	96.57	67.30	70.93	44.85	34.75	22.98	0.00	33.97	46.61	46.44
Visible	97.91	88.03	42.00	69.55	52.39	70.30	<u>76.72</u>	60.56	66.05	69.28
TarDAL	97.70	85.05	57.67	64.41	39.52	63.70	34.32	54.66	55.98	61.44
ReCoNet	97.55	83.95	56.54	58.69	35.54	59.52	69.24	45.33	46.03	61.38
LRRNet	98.29	89.60	68.34	69.06	49.64	71.14	76.51	61.17	64.82	72.06
MetaFusion	98.15	87.92	65.25	69.18	54.51	68.18	74.61	60.09	53.43	70.15
CDDFuse	98.47	90.10	74.13	72.00	<u>59.85</u>	71.72	76.16	61.58	65.54	74.40
DDFM	98.39	89.85	73.83	70.73	56.30	70.88	72.42	60.50	63.82	72.97
Text-IF	<u>98.49</u>	<u>90.16</u>	<u>74.60</u>	<u>72.12</u>	57.89	71.85	<b>76.98</b>	<u>62.59</u>	<b>70.38</b>	<u>75.01</u>
TextFusion	<u>98.27</u>	89.17	65.97	70.18	54.92	71.04	75.04	59.61	64.28	72.05
MMDRFuse	98.43	89.97	73.83	71.50	58.05	<u>72.04</u>	74.96	61.87	64.14	73.87
<b>Ours</b>	<b>98.53</b>	<b>90.55</b>	<b>74.86</b>	<b>72.27</b>	<b>60.70</b>	<b>72.42</b>	76.60	<b>62.62</b>	<u>69.86</u>	<b>75.38</b>

Table 3. Quantitative comparison of semantic segmentation performance on the MSRS dataset. The bolded values indicate the best performance, while underlined values represent the second-best.

Setting	EN $\uparrow$	SD $\uparrow$	SCD $\uparrow$	VIF $\uparrow$	$Q^{AB/F} \uparrow$
(a) w/o MGCA	7.366	51.690	1.576	<b>1.065</b>	<b>0.765</b>
(b) w/o TIVR	7.382	52.201	1.608	1.063	0.764
(c) w/o GAF	7.383	51.956	1.572	1.065	0.764
(d) <b>Ours</b>	<b>7.396</b>	<b>52.553</b>	<b>1.614</b>	1.059	0.763

Table 4. Quantitative ablation results on LLVIP dataset. The bolded values indicate the best performance.

tures. As Tab. 4 (b) shows, without text semantic guidance, the fused images exhibit noticeably poorer image information and texture details. This indicates that, in the absence of text guidance, the model struggles to effectively integrate crucial information from the images. Consequently, the fusion lacks detail, particularly in texture retention and semantic consistency. This experiment highlights the significance of text semantic guidance in enhancing the quality of the fused images.

**Effectiveness of the Gated Attentional Fusion (GAF) Module.** To investigate the impact of excluding the gating mechanism for dynamically learning multimodal features on fusion performance, we remove the GAF module and di-

rectly decode the initial fused features. As shown in Tab. 4 (c), this resulted in a significant decline in most evaluation metrics, emphasizing the importance of the GAF module. The GAF module dynamically adjusts the fusion weights of different modal features, effectively preserving rich information from both infrared and visible images while maintaining similarity to the source images, thereby significantly improving fusion quality.

## 5. Conclusion

In this paper, we propose TeSG, a novel method for infrared and visible image fusion that integrates textual semantic information. The method includes three core components: the Semantic Information Generator (SIG), the Mask-Guided Cross-Attention (MGCA) module, and the Text-Driven Attentional Fusion (TDAF) module. These components guide the fusion process to fully utilize both mask and text semantics, resulting in enhanced fused images. Extensive experimental results demonstrate the effectiveness of TeSG, showing significant improvements over existing state-of-the-art methods, particularly in terms of performance on downstream tasks such as object detection and semantic segmentation. Future work will explore more controllable fusion

mechanisms and broader applications of cross-modal information.

## References

- [1] FirstName Alpher. Frobnication. *IEEE TPAMI*, 12(1):234–778, 2002.
- [2] FirstName Alpher and FirstName Fotheringham-Smythe. Frobnication revisited. *Journal of Foo*, 13(1):234–778, 2003.
- [3] FirstName Alpher and FirstName Gamow. Can a computer frobnicate? In *CVPR*, pages 234–778, 2005.
- [4] FirstName Alpher, FirstName Fotheringham-Smythe, and FirstName Gamow. Can a machine frobnicate? *Journal of Foo*, 14(1):234–778, 2004.
- [5] V Aslantas. A new image quality metric for image fusion: The sum of the correlations of differences. *Aeu-International Journal of Electronics and Communications*, 69(12):1890–1896, 2015. 5
- [6] Durga Prasad Bavirisetti and Ravindra Dhuli. Two-scale image fusion of visible and infrared images using saliency detection. *Infrared Physics & Technology*, 76:52–64, 2016. 2
- [7] Liang-Chieh Chen, Yukun Zhu, George Papandreou, Florian Schroff, and Hartwig Adam. Encoder-decoder with atrous separable convolution for semantic image segmentation. In *Proceedings of the European Conference on Computer Vision*, pages 801–818, 2018. 7
- [8] Chunyang Cheng, Tianyang Xu, Xiao-Jun Wu, Hui Li, Xi Li, Zhangyong Tang, and Josef Kittler. Textfusion: Unveiling the power of textual semantics for controllable image fusion. *Information Fusion*, 117:102790, 2025. 2, 3, 5
- [9] Nedeljko Cvejic, David Bull, and Nishan Canagarajah. Region-based multimodal image fusion using ica bases. *IEEE Sensors Journal*, 7(5):743–751, 2007. 2
- [10] James W Davis and Vinay Sharma. Background-subtraction using contour-based fusion of thermal and visible imagery. *Computer Vision and Image Understanding*, 106(2-3):162–182, 2007. 1
- [11] Yanglin Deng, Tianyang Xu, Chunyang Cheng, Xiao-Jun Wu, and Josef Kittler. Mmdrfuse: Distilled mini-model with dynamic refresh for multi-modality image fusion. In *Proceedings of the 32nd ACM International Conference on Multimedia*, pages 7326–7335, 2024. 5
- [12] Ian J. Goodfellow, Jean Pouget-Abadie, Mehdi Mirza, Bing Xu, David Warde-Farley, Sherjil Ozair, Aaron Courville, and Yoshua Bengio. Generative adversarial nets. In *Proceedings of the 28th International Conference on Neural Information Processing Systems*, page 2672–2680, 2014. 2
- [13] Jungong Han, Eric J Pauwels, and Paul De Zeeuw. Fast saliency-aware multi-modality image fusion. *Neurocomputing*, 111:70–80, 2013. 1
- [14] Yu Han, Yunze Cai, Yin Cao, and Xiaoming Xu. A new image fusion performance metric based on visual information fidelity. *Information fusion*, 14(2):127–135, 2013. 5
- [15] Zhanbo Huang, Jinyuan Liu, Xin Fan, Risheng Liu, Wei Zhong, and Zhongxuan Luo. Reconet: Recurrent correction network for fast and efficient multi-modality image fusion. In *Proceedings of the European Conference on Computer Vision*, pages 539–555, 2022. 5
- [16] Xinyu Jia, Chuang Zhu, Minzhen Li, Wenqi Tang, and Wenli Zhou. Llvip: A visible-infrared paired dataset for low-light vision. In *Proceedings of the IEEE/CVF International Conference on Computer Vision*, pages 3496–3504, 2021. 5, 6, 8
- [17] Weiwei Kong, Yang Lei, and Huaixun Zhao. Adaptive fusion method of visible light and infrared images based on non-subsampled shearlet transform and fast non-negative matrix factorization. *Infrared Physics & Technology*, 67:161–172, 2014.
- [18] FirstName LastName. The frobnicable foo filter, 2014. Face and Gesture submission ID 324. Supplied as supplemental material fg324.pdf.
- [19] FirstName LastName. Frobnication tutorial, 2014. Supplied as supplemental material tr.pdf.
- [20] Guofa Li, Yongjie Lin, and Xingda Qu. An infrared and visible image fusion method based on multi-scale transformation and norm optimization. *Information Fusion*, 71:109–129, 2021. 2
- [21] Hui Li and Xiao-Jun Wu. Densefuse: A fusion approach to infrared and visible images. *IEEE Transactions on Image Processing*, 28(5):2614–2623, 2018. 2
- [22] He Li, Lei Liu, Wei Huang, and Chao Yue. An improved fusion algorithm for infrared and visible images based on multi-scale transform. *Infrared Physics & Technology*, 74: 28–37, 2016. 2
- [23] Hongguang Li, Wenrui Ding, Xianbin Cao, and Chunlei Liu. Image registration and fusion of visible and infrared integrated camera for medium-altitude unmanned aerial vehicle remote sensing. *Remote Sensing*, 9(5):441, 2017. 1
- [24] Hui Li, Xiao-Jun Wu, and Josef Kittler. Rfn-nest: An end-to-end residual fusion network for infrared and visible images. *Information Fusion*, 73:72–86, 2021. 2
- [25] Hui Li, Tianyang Xu, Xiao-Jun Wu, Jiwen Lu, and Josef Kittler. Lrrnet: A novel representation learning guided fusion network for infrared and visible images. *IEEE Transactions on Pattern Analysis and Machine Intelligence*, 45(9):11040–11052, 2023. 5
- [26] Junnan Li, Dongxu Li, Caiming Xiong, and Steven Hoi. Blip: Bootstrapping language-image pre-training for unified vision-language understanding and generation. In *Proceedings of the 39th International Conference on Machine Learning*, pages 12888–12900. PMLR, 2022. 2, 3, 4
- [27] Shutao Li, Xudong Kang, and Jianwen Hu. Image fusion with guided filtering. *IEEE Transactions on Image Processing*, 22(7):2864–2875, 2013. 2
- [28] CH Liu, Yue Qi, and WR Ding. Infrared and visible image fusion method based on saliency detection in sparse domain. *Infrared Physics & Technology*, 83:94–102, 2017. 2
- [29] Jinyuan Liu, Xin Fan, Ji Jiang, Risheng Liu, and Zhongxuan Luo. Learning a deep multi-scale feature ensemble and an edge-attention guidance for image fusion. *IEEE Transactions on Circuits and Systems for Video Technology*, 32(1): 105–119, 2021. 2

- [30] Jinyuan Liu, Xin Fan, Zhanbo Huang, Guanyao Wu, Risheng Liu, Wei Zhong, and Zhongxuan Luo. Target-aware dual adversarial learning and a multi-scenario multi-modality benchmark to fuse infrared and visible for object detection. In *Proceedings of the IEEE/CVF Conference on Computer Vision and Pattern Recognition*, pages 5802–5811, 2022. 2, 3, 5
- [31] Jinyuan Liu, Zhu Liu, Guanyao Wu, Long Ma, Risheng Liu, Wei Zhong, Zhongxuan Luo, and Xin Fan. Multi-interactive feature learning and a full-time multi-modality benchmark for image fusion and segmentation. In *Proceedings of the IEEE/CVF International Conference on Computer Vision*, pages 8115–8124, 2023. 3
- [32] Yu Liu, Xun Chen, Juan Cheng, Hu Peng, and Zengfu Wang. Infrared and visible image fusion with convolutional neural networks. *International Journal of Wavelets, Multiresolution and Information Processing*, 16(03):1850018, 2018. 2
- [33] Jinlei Ma, Zhiqiang Zhou, Bo Wang, and Hua Zong. Infrared and visible image fusion based on visual saliency map and weighted least square optimization. *Infrared Physics & Technology*, 82:8–17, 2017. 2
- [34] Jiayi Ma, Yong Ma, and Chang Li. Infrared and visible image fusion methods and applications: A survey. *Information fusion*, 45:153–178, 2019. 1, 5, 6
- [35] Jiayi Ma, Wei Yu, Pengwei Liang, Chang Li, and Junjun Jiang. Fusiongan: A generative adversarial network for infrared and visible image fusion. *Information fusion*, 48:11–26, 2019. 2
- [36] Jiayi Ma, Pengwei Liang, Wei Yu, Chen Chen, Xiaojie Guo, Jia Wu, and Junjun Jiang. Infrared and visible image fusion via detail preserving adversarial learning. *Information Fusion*, 54:85–98, 2020.
- [37] Jiayi Ma, Han Xu, Junjun Jiang, Xiaoguang Mei, and Xiaoping Zhang. Ddegan: A dual-discriminator conditional generative adversarial network for multi-resolution image fusion. *IEEE Transactions on Image Processing*, 29:4980–4995, 2020. 2
- [38] Jiayi Ma, Hao Zhang, Zhenfeng Shao, Pengwei Liang, and Han Xu. Ganmcc: A generative adversarial network with multiclassification constraints for infrared and visible image fusion. *IEEE Transactions on Instrumentation and Measurement*, 70:1–14, 2020. 2
- [39] Jiayi Ma, Linfeng Tang, Fan Fan, Jun Huang, Xiaoguang Mei, and Yong Ma. Swinfusion: Cross-domain long-range learning for general image fusion via swin transformer. *IEEE/CAA Journal of Automatica Sinica*, 9(7):1200–1217, 2022. 2
- [40] Mehdi Mirza and Simon Osindero. Conditional generative adversarial nets. *arXiv preprint arXiv:1411.1784*, 2014. 2
- [41] Jiaming Song, Chenlin Meng, and Stefano Ermon. Denoising diffusion implicit models. In *International Conference on Learning Representations*, 2021. 4
- [42] Linfeng Tang, Jiteng Yuan, and Jiayi Ma. Image fusion in the loop of high-level vision tasks: A semantic-aware real-time infrared and visible image fusion network. *Information Fusion*, 82:28–42, 2022. 3
- [43] Linfeng Tang, Jiteng Yuan, Hao Zhang, Xingyu Jiang, and Jiayi Ma. Piafusion: A progressive infrared and visible image fusion network based on illumination aware. *Information Fusion*, 83:79–92, 2022. 5, 6, 7
- [44] Hebaixu Wang, Hao Zhang, Xunpeng Yi, Xinyu Xiang, Leyuan Fang, and Jiayi Ma. Terf: Text-driven and region-aware flexible visible and infrared image fusion. In *Proceedings of the 32nd ACM International Conference on Multimedia*, pages 935–944, 2024. 2, 3
- [45] Jun Wang, Jinye Peng, Xiaoyi Feng, Guiqing He, and Jianping Fan. Fusion method for infrared and visible images by using non-negative sparse representation. *Infrared Physics & Technology*, 67:477–489, 2014. 2
- [46] Zhou Wang, Alan C Bovik, Hamid R Sheikh, and Eero P Simoncelli. Image quality assessment: from error visibility to structural similarity. *IEEE Transactions on Image Processing*, 13(4):600–612, 2004.
- [47] Zhishe Wang, Yanlin Chen, Wenyu Shao, Hui Li, and Lei Zhang. Swinfuse: A residual swin transformer fusion network for infrared and visible images. *IEEE Transactions on Instrumentation and Measurement*, 71:1–12, 2022. 2
- [48] Han Xu, Jiayi Ma, Junjun Jiang, Xiaojie Guo, and Haibin Ling. U2fusion: A unified unsupervised image fusion network. *IEEE Transactions on Pattern Analysis and Machine Intelligence*, 44(1):502–518, 2020. 2, 5, 6
- [49] Han Xu, Jiayi Ma, Jiteng Yuan, Zhuliang Le, and Wei Liu. Rfnnet: Unsupervised network for mutually reinforcing multimodal image registration and fusion. In *Proceedings of the IEEE/CVF Conference on Computer Vision and Pattern Recognition*, pages 19679–19688, 2022. 2
- [50] Philippe Xu, Franck Davoine, Jean-Baptiste Bordes, Huijing Zhao, and Thierry Denœux. Multimodal information fusion for urban scene understanding. *Machine Vision and Applications*, 27:331–349, 2016. 1
- [51] Xunpeng Yi, Han Xu, Hao Zhang, Linfeng Tang, and Jiayi Ma. Text-if: Leveraging semantic text guidance for degradation-aware and interactive image fusion. In *Proceedings of the IEEE/CVF Conference on Computer Vision and Pattern Recognition*, pages 27026–27035, 2024. 2, 3, 5
- [52] Jun Yue, Leyuan Fang, Shaobo Xia, Yue Deng, and Jiayi Ma. Dif-fusion: Toward high color fidelity in infrared and visible image fusion with diffusion models. *IEEE Transactions on Image Processing*, 32:5705–5720, 2023. 2
- [53] Hao Zhang and Jiayi Ma. Sdnet: A versatile squeeze-and-decomposition network for real-time image fusion. *International Journal of Computer Vision*, 129(10):2761–2785, 2021. 2
- [54] Hao Zhang, Han Xu, Xin Tian, Junjun Jiang, and Jiayi Ma. Image fusion meets deep learning: A survey and perspective. *Information Fusion*, 76:323–336, 2021. 1
- [55] Wenda Zhao, Shigeng Xie, Fan Zhao, You He, and Huchuan Lu. Metafusion: Infrared and visible image fusion via meta-feature embedding from object detection. In *Proceedings of the IEEE/CVF Conference on Computer Vision and Pattern Recognition*, pages 13955–13965, 2023. 5
- [56] Zixiang Zhao, Shuang Xu, Chunxia Zhang, Junmin Liu, Jianshe Zhang, and Pengfei Li. Didfuse: deep image de-

- composition for infrared and visible image fusion. In *Proceedings of the 29th International Conference on International Joint Conferences on Artificial Intelligence*, pages 976–976, 2021. [2](#)
- [57] Zixiang Zhao, Haowen Bai, Jianshe Zhang, Yulun Zhang, Shuang Xu, Zudi Lin, Radu Timofte, and Luc Van Gool. Cddfuse: Correlation-driven dual-branch feature decomposition for multi-modality image fusion. In *Proceedings of the IEEE/CVF Conference on Computer Vision and Pattern Recognition*, pages 5906–5916, 2023. [5](#)
- [58] Zixiang Zhao, Haowen Bai, Yuanzhi Zhu, Jianshe Zhang, Shuang Xu, Yulun Zhang, Kai Zhang, Deyu Meng, Radu Timofte, and Luc Van Gool. Ddfm: denoising diffusion model for multi-modality image fusion. In *Proceedings of the IEEE/CVF International Conference on Computer Vision*, pages 8082–8093, 2023. [2](#), [5](#)
- [59] Zixiang Zhao, Lilun Deng, Haowen Bai, Yukun Cui, Zhipeng Zhang, Yulun Zhang, Haotong Qin, Dongdong Chen, Jianshe Zhang, Peng Wang, et al. Image fusion via vision-language model. In *Proceedings of the 41st International Conference on Machine Learning*, pages 60749–60765, 2024. [2](#), [3](#)